

Towards eliminating the nonlinear Kelvin wake

J. S. Keeler* and M. G. Blyth†

School of Engineering, Mathematics and Physics, University of East Anglia, Norwich, NR4 7TJ, UK

B. J. Binder‡

School of Computer and Mathematical Sciences, University of Adelaide, Australia

The disturbance caused by a localised forcing moving at constant speed on the free surface of a liquid of finite depth is investigated using the forced Kadomtsev-Petviashvili equation. The presence of a steady v-shaped Kelvin wave pattern downstream of the forcing is established for this model equation, and the wedge angle is characterised as a function of the Froude number. It is shown that the wake can be eliminated via a careful choice of the forcing distribution and, moreover, that the corresponding wave-free solution is stable so that it could potentially be seen in a physical experiment. The stability is demonstrated via the numerical solution of an initial value problem for which the steady wave-free state is attained in the long-time limit.

I. INTRODUCTION

The study of the wake produced by a moving body on the surface of water is a classical problem in fluid dynamics. The v-shaped wake pattern that is seen behind such a body is a rare example of a fluid dynamics phenomenon that is well-known to everyone. Attempting to minimise or even eliminate the Kelvin wake presents an important problem since in many applications its presence leads to undesirable consequences. For example it can cause erosion to waterway and river banks [e.g. 1], and the wave drag it produces limits the fuel efficiency of boats and ships [5].

The mathematical description of the three-dimensional Kelvin wake has been well known for over a century [9]. Typically, a moving body such as a ship is represented by a pressure disturbance that propagates over the fluid surface. The angle subtended by the characteristic v-shape bounding the main surface disturbance is usually referred to as the Kelvin wedge angle, and is herein denoted by θ_k . In deep water θ_k can be found using a linear simplification of the full Euler system on the assumption that the disturbance to the surface is small. This leads to the result that $\tan^2 \theta_k = 1/8$ yielding $\theta_k \approx 19.47^\circ$ [see, for example 22]. In shallow water θ_k depends on the flow-speed and water depth [18].

Despite the ubiquity of the Kelvin wake phenomenon, and the large number of research articles that have been devoted to it, it remains a topic of considerable scientific interest. We highlight in particular two research areas of recent interest: (i) the numerical calculation of the fully nonlinear Kelvin wake and the associated wave-drag, and (ii) the theoretical description of Kelvin wakes for slow-moving vessels. For (i) the so-called ‘wave-drag coefficient’ [5, 11, 15] can be used to quantify the resistance induced by the wake. Recently, [2, 16, 21] used a numerical boundary-integral approach coupled with Newton-Krylov and pre-conditioning techniques to solve the fully nonlinear Euler system for inviscid, irrotational flow (hereinafter referred to as the Euler system) in order to capture efficiently the steady wave patterns behind a moving object, and provided important insight into the nonlinear wave-drag. Significantly, [2, 16] showed that as the flow-speed and forcing pressure amplitude are increased, nonlinearity, via the amplitude of the external forcing, alters the Kelvin wedge angle and therefore the physical extent of the wavy region. In the aforementioned studies, the authors made simple choices for the external forcing functions, for example using combinations of Gaussian forcing functions. There has also been work done to quantify the wave-drag for an arbitrary forcing distribution using the linearised form of the Euler system [13]. In none of these studies did the wave-pattern completely disappear for any choice of the external forcing.

Regarding (ii), for slow-moving boats the Froude number, $Fr = U/\sqrt{gH}$, is small, where U , g and H are a typical flow speed, the gravitational acceleration, and a typical length scale, respectively. Assuming $Fr \ll 1$, an asymptotic solution of the two-dimensional Euler system that utilises expansions in powers of Fr , somewhat surprisingly, produces no waves at each order of Fr . This apparent paradox can be resolved by resorting to ‘beyond-all-orders’ asymptotics, and in this context it can be shown that there are waves present downstream that are exponentially small in Fr [19, 20]. For the two-dimensional problem, [20] showed that downstream waves cannot be eliminated for a single-cornered ship. However, [19] were not able to make such a conclusive statement for more general piecewise-linear hulls and they did not discount the possibility of wave-free solutions. [12] and [17] considered the linear three-dimensional problem and characterised the wedge angle in terms of the system parameters. Recently, as a first step towards examining the Euler system, [7] showed how an exponential asymptotics approach may be used for smooth boat hulls in the context of a model equation. Examining smooth hulls is important as they can be used to model the

* j.keeler@uea.ac.uk

† m.blyth@uea.ac.uk

‡ benjamin.binder@adelaide.edu.au

bulbous hull shapes that are known to minimise wave-drag [see, for example 4]. However, modelling smooth bodies moving at arbitrary speeds using the Euler system remains an open challenge.

In this paper, we work towards the goal of eliminating the Kelvin wake behind a moving body in a real flow by studying the simplified model Kadomtsev-Petviashvili equation with a localised forcing term. This equation was originally derived by [8], and it is hereinafter referred to as fKP. We demonstrate that for this equation a generic forcing produces a trailing wave pattern that is similar to that found for the Euler system with a v-shaped wake whose angle we characterise as a function of the Froude number. This includes the critical case $Fr = 1$ covered by [8], who showed that under this condition the wake fills the entire region behind the disturbance. Furthermore, we use a simple mathematical argument to show that for the fKP system it is possible to eliminate the wake. By a judicious choice of forcing function, we construct solutions for which the disturbance to the water surface is localised around the forcing so that the surface is undisturbed in all directions into the far field. We refer to such solutions as *wave-free* solutions. Strikingly, we provide evidence that the wave-free solutions are stable, meaning that they are reached in the long-time limit of an initial value problem (IVP), leading to the possibility of observing them in a physical experiment.

We proceed as follows. In § II we describe the problem statement including the fKP equation and boundary conditions, and we characterise the v-shaped Kelvin wake-pattern that emerges for a generic choice of forcing function. In § III we discuss how to construct a wave-free steady state for the fully nonlinear fKP equation in the presence of a suitably chosen localised forcing. In § IV we formulate and solve numerically an IVP to show that the wave-free states are stable. Finally, in § V we present our conclusions and highlight future directions for study.

II. STEADY KELVIN WAKE-PATTERNS OF THE fKP

Before we demonstrate how we construct wave-free solutions, it is instructive to characterise the v-shaped Kelvin wake-pattern, and in particular the wedge angle, for a generically chosen external forcing in terms of the flow-speed. The procedure we follow is well known for the Euler system [see, for example 13] and has recently been reconstructed for a different model PDE (partial differential equation) by [7].

As derived in the context of water-waves the fKP is a PDE for the height of the free-surface, denoted $\eta(\mathbf{x}, t)$, in terms of an external forcing profile, $\sigma(\mathbf{x})$ (either representing a surface pressure distribution or the shape of a topographic obstacle), where $\mathbf{x} = [x, y]^T$ and the prevailing flow is in the x direction [8]. It is derived from the Euler system under the assumptions of i) shallow-water, ii) small forcing amplitude, iii) weak y -dependence and iv) $Fr \approx 1$ [see, for example 10, for mathematically rigorous statements on the validity of this model]. Therefore, in contrast to the small- Fr literature stated in the introduction, our system describes moderate and fast-moving boats/topographic obstacles. The equation is

$$\left(\eta_t + (Fr - 1)\eta_x - \frac{3}{2}\eta\eta_x - \frac{1}{6}\eta_{xxx} - \frac{1}{2}\sigma_x \right)_x - \frac{1}{2}\eta_{yy} = 0, \quad x, y \in \mathbb{R}, \quad (1)$$

where the subscripts indicate partial derivatives. Far upstream of the forcing, the free-surface is assumed flat and hence we impose the boundary conditions

$$\eta, \eta_x, \eta_{xx}, \eta_{xxx} \rightarrow 0, \quad \text{as } x \rightarrow -\infty, \quad (2)$$

$$\eta_y \rightarrow 0, \quad \text{as } y \rightarrow \pm\infty. \quad (3)$$

We note that (1) is valid in the context of no/weak surface tension, and is a modification of the KP-II equation (the KP-I equation has the opposite sign on the fourth derivative and is for strong surface tension). We emphasise that we were unable to find any explicit analysis for the Kelvin wedge angle in (1) in the literature, but note the linear analysis of [8]; restricted to critical flow, $Fr = 1$, and a time-dependent response with no explicit determination of the Kelvin wedge angle as a function of Fr .

To determine the Kelvin wedge angle, we examine linear steady solutions to (1) by assuming η is small;

$$\mathcal{L}(\eta_\ell) = 3\sigma_{\ell,xx}, \quad \mathcal{L} \equiv 6(Fr - 1)\partial_{xx} - \partial_{xxx} - 3\partial_{yy} = 0. \quad (4)$$

For convenience, in what follows, η_ℓ, σ_ℓ correspond to a linear solution and forcing term of (4), while η, σ correspond to a nonlinear solution and forcing term of (1).

We solve (4) using the two-dimensional Fourier transform, defined as

$$\hat{\eta}_\ell(\mathbf{k}) = \mathcal{F}(\eta_\ell) \equiv \frac{1}{2\pi} \int_{-\infty}^{\infty} \int_{-\infty}^{\infty} \eta_\ell(\mathbf{x}) \exp(-i\mathbf{k} \cdot \mathbf{x}) \, dx \, dy, \quad (5)$$

where $\mathbf{k} = [k_x, k_y]^T$. Introducing a polar coordinate system;

$$\mathbf{x} = r[\cos \theta, \sin \theta]^T, \quad \mathbf{k} = \kappa[\cos \varphi, \sin \varphi]^T \quad (6)$$

and letting $\hat{\sigma}_\ell(\mathbf{k}) = \mathcal{F}(\sigma)$, the steady linear solution to (4) can be written in terms of the inverse Fourier transform as

$$\eta_\ell(\mathbf{x}) = \frac{1}{2\pi} \int_0^{2\pi} \int_0^\infty \frac{3\hat{\sigma}_\ell(\mathbf{k}) \kappa \exp(i\kappa r \cos(\varphi - \theta))}{(\kappa^2 - \kappa_0^2) \cos^2 \varphi} d\kappa d\varphi, \quad \kappa_0^2 = \frac{3 \tan^2 \varphi - 6(Fr - 1)}{\cos^2 \varphi}. \quad (7)$$

The Kelvin wedge angle can be determined by examining the leading-order asymptotic behaviour of (7) far downstream, as $r \rightarrow \infty$, $|\theta| < \pi/2$. To proceed, the inner κ -integration can be achieved by extending the domain of integration into the complex plane, i.e. $\kappa \in \mathbb{C}$, and then using Cauchy's residue theorem. For subcritical and critical flow, $Fr < 1$ and $Fr = 1$, respectively, $\kappa_0^2 > 0$, and hence there are simple poles at $\kappa = \pm\kappa_0$; we only consider the pole at $\kappa = +\kappa_0$ as the integration limits in (7) is the positive real line. If $Fr > 1$, it is possible that $\kappa_0^2 < 0$ and this will be discussed below.

Great care has to be taken when choosing the path of integration and choice of contour indentation around the pole $\kappa = +\kappa_0$. For $\cos(\varphi - \theta) > 0$, we close our path of integration in the upper half complex κ -plane by adding a quarter-circle arc from the positive real κ axis to the positive imaginary κ axis and then returning back to the origin (we note that the contribution of the integrand on the imaginary axis is exponentially small in r). The boundary conditions, (2), dictate there are no waves far upstream and hence if $\cos \theta < 0$ ($x < 0$) we indent the contour on the real κ -axis so it goes over the pole and hence make no contribution to the integral. Far downstream, when $\cos \theta > 0$, when waves can appear due to the radiation condition, the contour is indented under the pole; therefore making a non-zero contribution due to the residue of the integrand at κ_0 . For supercritical flow, $Fr > 1$, κ_0^2 will become negative when $\tan^2 \varphi < 2(Fr - 1)$ and the pole will be located on the imaginary axis, but in this case the residue is now exponentially small as $r \rightarrow \infty$. We note that for $\cos(\varphi - \theta) < 0$ the contour gets deformed onto the negative imaginary axis and the preceding description of the contour is reversed.

Assuming $\cos \theta > 0$ and the pole is on the real axis if $Fr > 1$, by calculating the residue of the pole, the leading-order asymptotic behaviour far downstream is

$$\eta_\ell(\mathbf{x}) \sim \frac{3}{2} \mathbf{i} \int_{-\pi/2+\theta}^{\pi/2} \frac{\hat{\sigma}_\ell(\mathbf{k}_0)}{\cos^2 \varphi} \exp(i|\kappa_0|r \cos(\varphi - \theta)) d\varphi, \quad \text{as } r \rightarrow \infty, \quad (8)$$

where $\mathbf{k}_0 = |\kappa_0|[\cos \varphi, \sin \varphi]^T$ is dependent on φ only. The limits of integration on the outer- φ integral have changed from (7) as the solution is symmetric about $\theta = 0$ so we only need to consider $0 < \theta < \pi$, which means that as $\cos(\varphi - \theta) > 0$, $-\pi/2 + \theta < \varphi < \pi/2$ (if $\cos(\varphi - \theta) < 0$ then $-\pi/2 < \varphi < \pi/2 - \theta$). The dominant behaviour of the integral as $r \rightarrow \infty$ occurs when the exponent in (8) is stationary, i.e.

$$\frac{\partial g}{\partial \varphi} = 0, \quad \text{where } g(\varphi, \theta) = \kappa_0 \cos(\varphi - \theta) \equiv \frac{\sqrt{3}(\tan^2 \varphi - 2(Fr - 1))^{1/2} \cos(\varphi - \theta)}{\cos \varphi}, \quad (9)$$

The leading-order asymptotic behaviour of (8) as $r \rightarrow \infty$ is readily obtained using the stationary-phase formula

$$\eta_\ell(\mathbf{x}) \sim \frac{3\sqrt{\pi}(\mathbf{i} - \lambda)}{4} \sum_n r^{-1/2} \frac{\hat{\sigma}_\ell(\mathbf{k}_0, \varphi_n)}{|g''(\varphi_n)|^{1/2} \cos^2 \varphi_n} \exp[i|\kappa_0|r \cos(\varphi_n - \theta)] + \text{c.c.}, \quad (10)$$

where the sum is over the n permissible solutions, $\varphi = \varphi_n$, of (9), $\lambda = \text{sgn}(g''(\varphi_n))$ is the signum function, $g''(\varphi_n)$ is the second derivative of $g(\varphi)$ with respect to φ , $\hat{\sigma}_\ell(\mathbf{k}_0, \varphi_n) = \hat{\sigma}_\ell(\mathbf{k}_0)|_{\varphi=\varphi_n}$ and c.c stands for complex conjugate. Physically, as can be seen from (10), κ_0 characterises the wave number of the oscillations far downstream.

When $Fr = 1$ (9) has a unique solution, $\varphi = \varphi_1$, for any $0 < |\theta| < \pi/2$ which satisfies

$$\tan \varphi = -\frac{1}{2} \cot \theta. \quad (11)$$

This solution exists for all $0 < |\theta| < \pi/2$ and hence the Kelvin wedge angle is $\theta_k = \pi/2$, as was first noted in [8]. Substituting φ_1 into (10) produces a so-called *divergent* wave profile for η_ℓ . A key feature of divergent waves is the presence of a 'shadow-region' downstream of the forcing where there is no surface disturbance, see figure 1(b). To see this, $\varphi_1 \rightarrow -\pi/2$ and $\kappa_0 \rightarrow \infty$ as $\theta \rightarrow 0$, see figure 1(e),(h). Therefore, examining (10), for a fixed value of $r \gg 1$; η_ℓ decays to zero as $\theta \rightarrow 0$, provided $\hat{\sigma}_\ell(\mathbf{k}_0, \varphi_1)$ decays sufficiently quickly as $\kappa_0 \rightarrow \infty$.

When $Fr \neq 1$ the solutions satisfy the quadratic equation for $\tan \varphi$,

$$2 \sin \theta \tan^2 \varphi + \cos \theta \tan \varphi - 2(Fr - 1) \sin \theta = 0. \quad (12)$$

Hence when $Fr < 1$ there are two real solutions for φ provided that

$$0 < |\theta| < \theta_k(Fr), \quad \text{where} \quad 16(1 - Fr) \tan^2 \theta_k = 1. \quad (13)$$

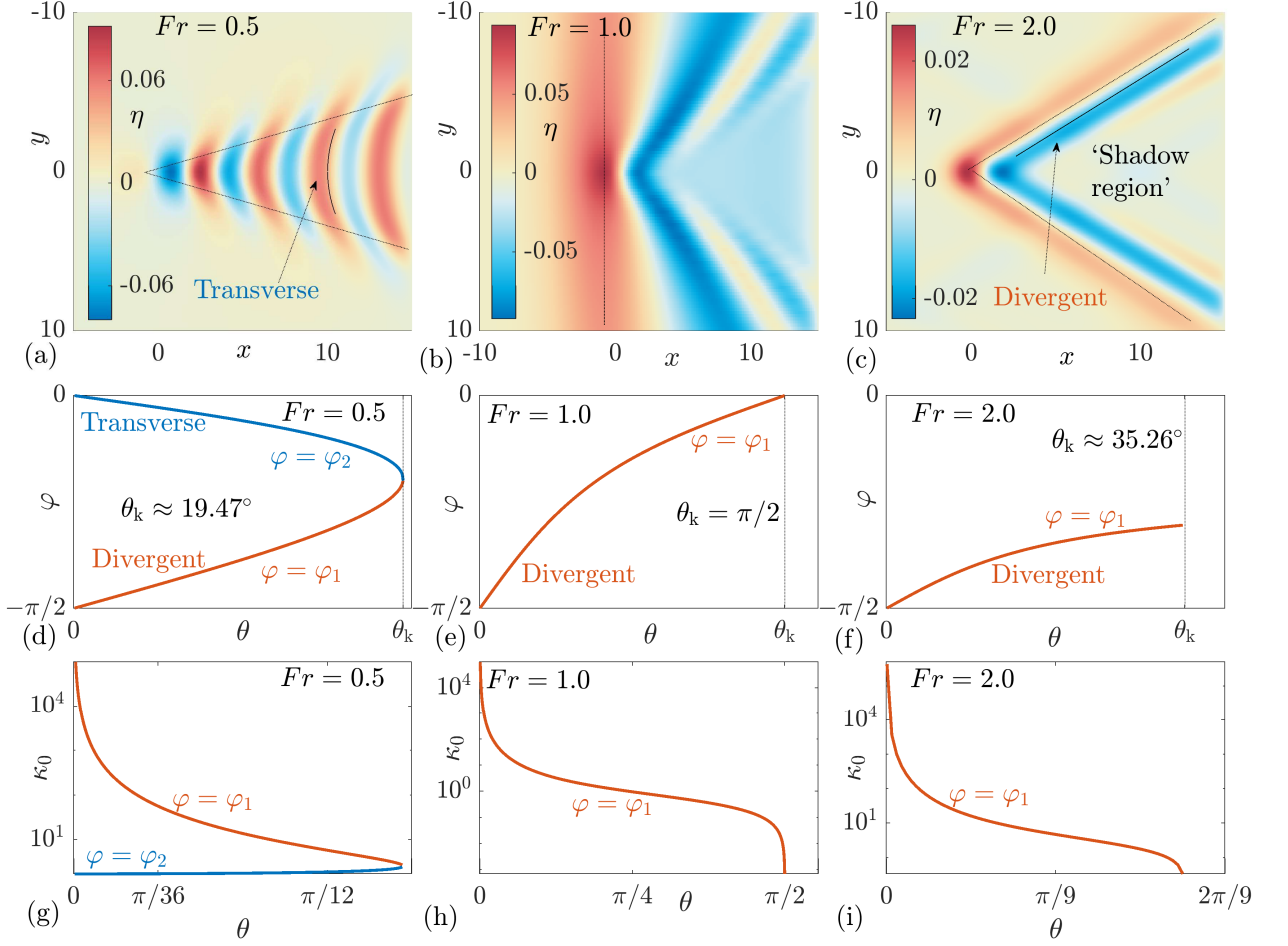


FIG. 1: The left, middle and right columns show results for $Fr = 0.5, 1.0$ and 2.0 , respectively. (a)-(c) Nonlinear steady solutions of (1) for $\sigma(\mathbf{x}) = a \exp(-\mathbf{x} \cdot \mathbf{x})$ with $a = 0.1$. The linear Kelvin wedge angle, θ_k is indicated as dotted lines. (d)-(f) The roots of (9) in the range $-\pi/2 + \theta < \varphi < \pi/2$ as a function of θ . (g)-(i) The pole on the real axis, κ_0 , evaluated at $\varphi_{1,2}$, as a function of θ .

The value of $\theta_k(Fr)$ is interpreted as the Kelvin wedge angle. It is indicated by the dashed vertical line in figure 1(d) for the case $Fr = 0.5$. Comparing the value of κ_0 at each root, see figure 1(g), we see that one of the solutions, φ_1 , is short-wavelength and corresponds to a divergent wave. The other solution, φ_2 , is long-wavelength and corresponds to a so-called *transverse* wave that does not decay to zero as $\theta \rightarrow 0$, for a fixed value of $r \gg 1$. In this case, no ‘shadow-region’ is present behind the forcing. For historical context, the divergent/transverse terminology was first coined in [6]. We note the special case of $Fr = 1/2$, as shown in figure 1(d),(g), which results in $\theta_k = \arctan(1/2\sqrt{2}) \approx 19.47^\circ$, the classical Kelvin wedge angle for the linearised Euler system. Interestingly, this is the value of Fr reported by [18] as approximately the transition point between a Kelvin wake-regime and a Mach wake-regime, where all linear waves travel with equal speed.

When $Fr > 1$ equation (12) has two solutions for any $0 < |\theta| < \pi/2$. However, for one of these solutions, φ_2 , we find that $\kappa_0^2 < 0$ for all $0 < |\theta| < \pi/2$ and so the pole in (7) is not on the real axis and does not contribute to the far-field wave pattern. For the other (divergent) solution, φ_1 , the transition from $\kappa_0^2 > 0$ (pole on the real axis) to $\kappa_0^2 < 0$ (pole on the imaginary axis) occurs when $\tan^2 \varphi = 2(Fr - 1)$. Inserting the latter into (12) we find that the permissible θ are bounded by the Kelvin wedge angle, θ_k and satisfies

$$0 < |\theta| < \theta_k(Fr), \quad \text{where} \quad 2(Fr - 1) \tan^2 \theta_k = 1. \quad (14)$$

In summary, we have determined the far-field Kelvin wedge angle as a function of Fr for subcritical and supercritical flow, as stated in (13) and (14), respectively. The wedge angle is plotted against Fr in figure 2. We note that $\theta_k \rightarrow \pi/2$ as $Fr \rightarrow 1^\pm$ and that for large Fr we have the asymptotic behaviour

$$\theta_k \sim (\sqrt{2}/2) Fr^{-1/2} \quad \text{as} \quad Fr \rightarrow \infty. \quad (15)$$

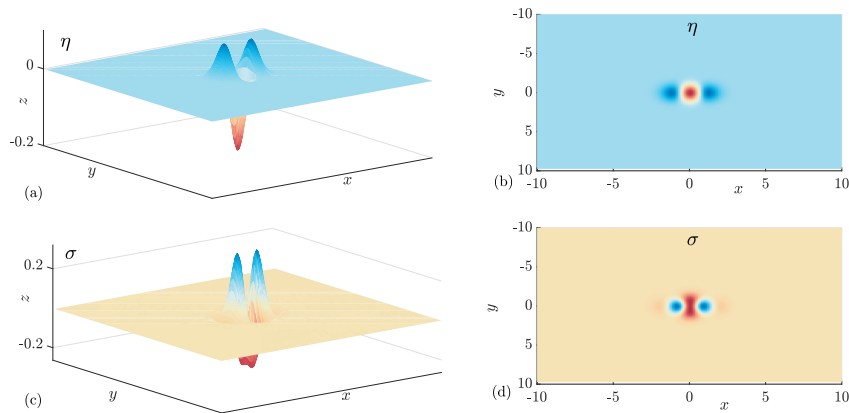


FIG. 2: Kelvin wedge angle dependence on Fr using (13) and (14).

For the Euler system and linearised Euler system, the dependence of the flow-speed on θ_k has been reported before, where it was found that increasing the forcing amplitude has the effect of increasing the wake angle beyond the classical Kelvin value [16], but increasing the flow-speed has effect of decreasing the wake angle [18]. The leading-order asymptotic behaviour in (15) differs to the $\theta_k \sim (\sqrt{2}/4\sqrt{\pi}) Fr^{-1}$ predicted by [13, 18]. This discrepancy can be explained by the fact that the fKP is only valid around $Fr \approx 1$.

We can compare the values obtained from the solution to (13) and (14) with the numerically computed nonlinear steady wave-patterns, found by solving the steady form of (1), as shown in figure 1(a)-(c) for $Fr = 0.5, 1.0, 2.0$, respectively. For concreteness, we choose a Gaussian forcing $\sigma(\mathbf{x}) = a \exp(-\mathbf{x} \cdot \mathbf{x})$ and $a = 0.1$. The dashed lines in each panel indicate the Kelvin wedge angle, θ_k . This theoretically derived angle shows excellent agreement with the numerically produced nonlinear wave patterns, giving us confidence in our numerical scheme (based on a variational formulation of (1) and discretised using finite-elements). Furthermore, the wave-patterns are qualitatively the same as the fully nonlinear solutions reported in [2], where transverse waves are present for $Fr < 1$ but absent when $Fr > 1$, where instead a ‘shadow-region’ appears.

To our knowledge this is the first time the Kelvin wedge angle and wave-pattern has been calculated explicitly for a range of Fr , in the context of the fKP equation and is the first main result of this paper. Due to the simplicity of (4), this demonstrates the promising potential of the fKP equation as a ‘sand-pit’ model to understand nonlinear Kelvin wave-patterns.

An important part of the analysis that we emphasise, is the importance of the pole, κ_0 , in producing waves downstream; if we can eliminate this pole then there is a possibility a wave-free steady state could exist. Since κ_0 does not depend on the explicit form of the forcing term, $\sigma(\mathbf{x})$, then the forcing does not play a leading role in determining the wave-pattern far downstream. It is often convenient to model $\sigma(\mathbf{x})$, taking the role as a ‘boat’, as a Dirac-delta function or Gaussian for a one-point wavemaker [see, for example 8, 22] or as a dipole modelling a two-point wavemaker [13, 14]. We will now show that through a judicious choice of $\hat{\sigma}(\mathbf{k})$, corresponding to a localised forcing term, a nonlinear steady wave-free $\eta(\mathbf{x})$ exists.

III. NONLINEAR WAVE-FREE STEADY SOLUTIONS

Initially, we concentrate on the linear solution (7), which in Cartesian coordinates ($\mathbf{k} = [k_x, k_y]^T$) can be written as

$$\eta_\ell(\mathbf{x}) = \frac{1}{2\pi} \int_{-\infty}^{\infty} \int_{-\infty}^{\infty} \frac{3k_x^2 \hat{\sigma}_\ell(\mathbf{k})}{6(Fr - 1)k_x^2 + k_x^4 - 3k_y^2} \exp(i\mathbf{k} \cdot \mathbf{x}) dk_x dk_y. \quad (16)$$

As previously stated, the pole in the integrand is responsible for the far-field wave pattern as $x \rightarrow \infty$. Therefore, an obvious choice for $\hat{\sigma}_\ell(\mathbf{k})$ that eliminates this pole is

$$\hat{\sigma}_\ell(\mathbf{k}) = \frac{1}{3} [6(Fr - 1)k_x^2 + k_x^4 - 3k_y^2] \hat{f}(\mathbf{k}), \quad (17)$$

where \hat{f} is the Fourier transform of an arbitrary function, $f(\mathbf{x})$, that is localised in physical space. Therefore, in physical space, the linear solution is

$$\eta_\ell(\mathbf{x}) = \frac{1}{2\pi} \int_{-\infty}^{\infty} \int_{-\infty}^{\infty} k_x^2 \hat{f}(\mathbf{k}) \exp(i\mathbf{k} \cdot \mathbf{x}) dk_x dk_y \equiv (f(\mathbf{x}))_{xx}. \quad (18)$$

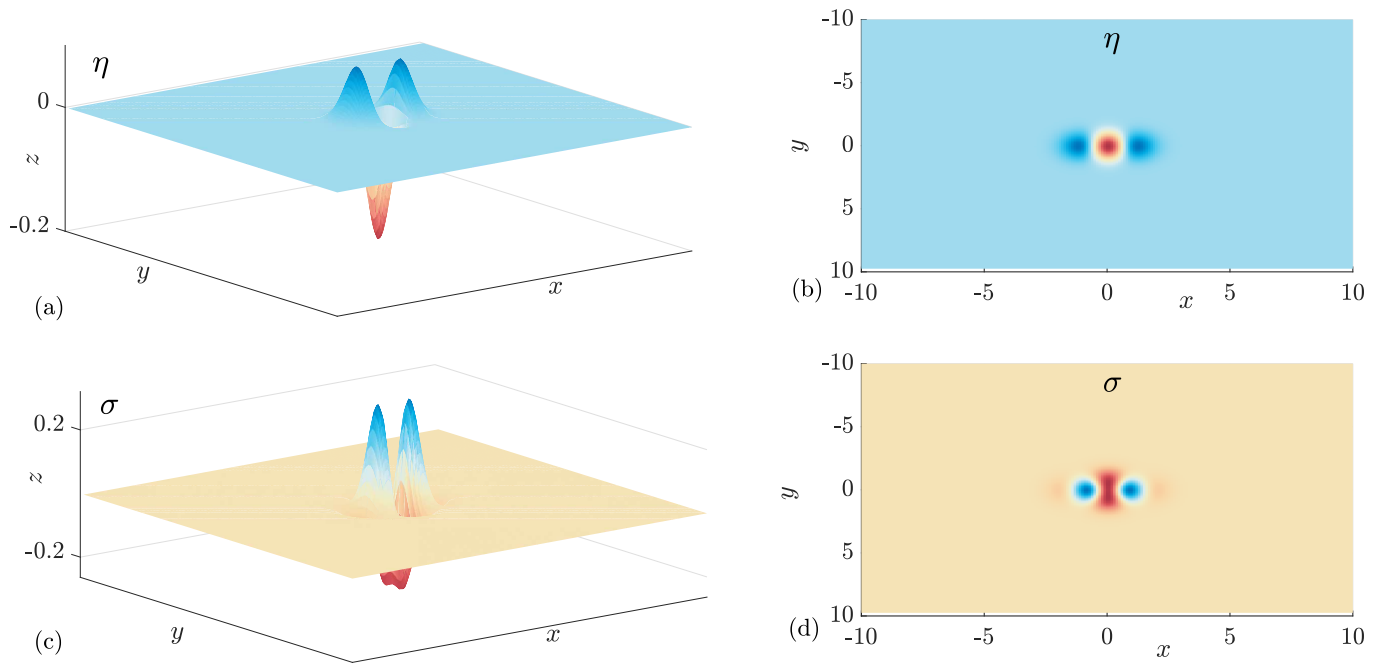


FIG. 3: Steady nonlinear wave-free solutions defined in (20). Panels (a)-(b); the nonlinear free-surface, $\eta(\mathbf{x})$ for $a = 0.1, Fr = 1.0$. Panels (c)-(d); the forcing, $\sigma(\mathbf{x})$.

A simple illustrative example is the choice $\hat{f}(\mathbf{k}) = -a \pi \exp(-(1/4)\mathbf{k} \cdot \mathbf{k})$, $a \in \mathbb{R}$. In this case it is straightforward to see from (18) that

$$\eta_\ell(\mathbf{x}) = a (\exp(-\mathbf{x} \cdot \mathbf{x}))_{xx}, \quad (19)$$

which is, crucially, wave-free in the far-field; thus achieving our goal. In the results that follow we concentrate on the example highlighted above in (19). Recall that η_ℓ and σ_ℓ satisfy (4) so, in order to satisfy the nonlinear problem (1), we choose

$$\eta(\mathbf{x}) = \eta_\ell(\mathbf{x}), \quad \sigma(\mathbf{x}) = \sigma_\ell(\mathbf{x}) - \frac{3}{2}\eta_\ell^2(\mathbf{x}). \quad (20)$$

As an example, when $a = 0.1, Fr = 1.0$, the nonlinear solutions η and σ in (20) are shown in figure 3 panels (a),(b) and (c),(d), respectively. This is our second result of the paper; we can choose a localised forcing function that results in a nonlinear wave-free, localised free-surface.

The forcing distribution in (20) is multi-signed which is similar to the dipole model of a monohull used by [14] and for more arbitrary pressure shapes in [13]. Although it is not difficult to determine the solution in (20) without resorting to a Fourier analysis, the strategy of eliminating the pole in the linear system does hint at a possible approach for minimising the waves in the Euler system, where the nonlinearity is not as straightforward as the quadratic term in (1). Finally we note that the steady free surface profile is sensitive to the choice of forcing in the sense that only a minor modification to (20) will lead to the reappearance of the Kelvin wake.

IV. STABILITY OF NONLINEAR WAVE-FREE STEADY SOLUTIONS

We now examine the solutions of (1) with (20) as the forcing term and (19) as the steady state. To probe the stability properties we solve a suite of IVPs numerically. We choose the initial condition

$$\eta(\mathbf{x}, t = 0) = 0, \quad (21)$$

which represents a flat free-surface. To benchmark our results, initially we solve the IVP with a Gaussian forcing function, $\sigma(\mathbf{x}) = a \exp(-\mathbf{x} \cdot \mathbf{x})$ and a dipole forcing $\sigma(\mathbf{x}) = a (\exp(-\mathbf{x} \cdot \mathbf{x}))_x$ ($a = 0.001$) and confirm that the system evolves towards a steady nonlinear Kelvin-wake, see movie_1.mp4 and movie_2.mp4 in the supplementary material.

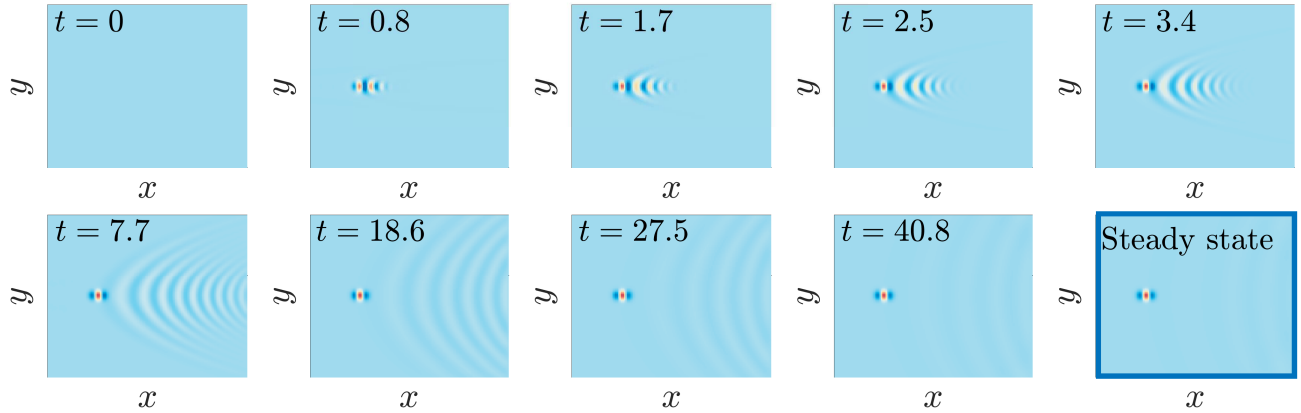


FIG. 4: Time-dependent nonlinear solution, $x \in [-10, 30]$, $y \in [-20, 20]$, starting from (21) with forcing in (19), $Fr = 1.0$, $a = 0.1$. The corresponding animation is shown in `movie_3.mp4` in the supplementary material.

Now, we concentrate on our special form of forcing in (19) and, to be consistent with the steady results in figure 3, choose $Fr = 1.0$, $a = 0.1$. Figure 4 (corresponding to the animation `movie_3.mp4` in the supplementary material) show the resulting time-dependent behaviour starting from (21). As can be seen from the time-snapshots, for approximately $0 < t < 7.7$ (top row) a curved wave pattern emerges directly downstream of the forcing. Then, for approximately $t \geq 7.7$ (bottom row) this wake-pattern propagates downstream in the form of curved ‘ripples’ before eventually separating and leaving the steady state, $\eta(\mathbf{x}, t)$ which we have confirmed is the steady state in (20). This behaviour is generic for a wide range of parameter space ($Fr \in [0.2, 1.8]$ and $a \in [-0.1, 0.1]$) and has been thoroughly checked for numerical convergence. This is strong numerical evidence that the wave-free steady state is not only stable but is also the asymptotic state of the system as $t \rightarrow \infty$. Furthermore, the waves emitted downstream in the initial stage of evolution appear different to the classical Kelvin wake-pattern and these ‘ripples’ may be linked to the recent work of [23], where ripple-solutions were reported for the unforced KP equation. As well as the initial condition in (21), the steady state is also stable to two- and three-dimensional perturbations as shown in `movie_4.mp4` and `movie_5.mp4`. Viewed altogether, these calculations show the remarkable stability of the wave-free steady state; our third, and perhaps most significant result of the paper. A carefully constructed forcing term, as described in the previous section, will result in a wave-free profile that can be observed in a physical experiment.

V. CONCLUSIONS AND PERSPECTIVE

We have demonstrated that the locally-forced Kadomtsev-Petviashvili (fKP) equation is capable of producing the v-shaped Kelvin wave pattern that is observed in practice when an object moves along the surface of water, and we have characterised the associated wedge angle as a function of the Froude number. More importantly we have shown that, for this system, a judiciously chosen forcing can produce a steady wave-free surface profile, meaning that the disturbance caused by the forcing is confined to its neighbourhood so that the surface is flat in the far-field. Crucially, using numerical simulations we have demonstrated that the wave-free states are stable in the sense that they are reached in the long-time limit of a suitably posed initial value problem.

Despite the simplicity of our mathematical argument, this appears to be the first time that wave-free steady solutions have been constructed for the fKP system and their stability properties calculated. Our results provide some evidence that it may be possible to eliminate the Kelvin wake in a real world setting. However, further work is needed to establish whether similar results can be achieved for other model systems or for the fully nonlinear Euler system, and whether wave-free solutions can be observed in a laboratory experiment. On the latter point, we highlight the interesting recent work by [3] in which asymmetric wake patterns have been observed experimentally.

Regarding applications, our results are at this point only suggestive. Nevertheless, they may ultimately pave the way to improving marine vessel design including the reduction of wave drag and the minimisation of the wake signature, as is desirable for ‘stealth’ boats, for example. The localised forcing in our system may also be treated as a model for a topographic feature on the bottom, in which case our wave-free solutions suggest the possibility of designing underwater structures that minimise or eliminate any disruption to the water surface.

For the fKP problem studied here, the free-surface profile is extremely sensitive to small changes in the forcing function, and we therefore anticipate that the forcing that produces wave-free solutions for fKP may not work so well for other model equations (e.g. the Green-Naghdi equations) or for the full Euler system. While various pressure distributions have been investigated for

the linearised Euler system [13], the fully nonlinear Euler system presents a considerable challenge, and is the subject of our ongoing work.

-
- [1] BISHOP, M. J. 2004 A posteriori evaluation of strategies of management: the effectiveness of no-wash zones in minimizing the impacts of boat-wash on macrobenthic infauna. *Environ. Manage.* **34** (1), 140–149.
- [2] BUTTLE, N. R., PETHIYAGODA, R., MORONEY, T. J. & McCUE, S. W. 2018 Three-dimensional free-surface flow over arbitrary bottom topography. *J. Fluid Mech.* **846**, 166–189.
- [3] EUVE, L-P., MAUREL, A., PETITJEANS, P. & PAGNEUX, V. 2024 Asymmetrical wakes over anisotropic bathymetries. *J. Fluid. Mech. Rap.* **984**, R6.
- [4] GROSENBAUGH, M. A. & YEUNG, R. W. 1989 Nonlinear bow flows-an experimental and theoretical investigation. In *Seventeenth Symposium on Naval Hydrodynamics*, pp. 195–213.
- [5] HAVELOCK, T. H. 1908 The effect of shallow water on wave resistance. *Proc. Roy. Soc. A* **100**, 499–505.
- [6] HAVELOCK, T. H. 1908 The propagation of groups of waves in dispersive media, with application to waves on water produced by a travelling disturbance. *Proc. Roy. Soc. A* **80**, 398–430.
- [7] KATAOKA, T. & AKYLAS, T.R. 2023 Nonlinear Kelvin wakes and exponential asymptotics. *Physica D* **454**, 133848.
- [8] KATSIS, C. & AKYLAS, T. R. 1987 On the excitation of long nonlinear water waves by a moving pressure distribution. part 2. three-dimensional effects. *J. Fluid Mech.* **177**, 49–65.
- [9] KELVIN, LORD 1887 On ship waves. *Proc. Inst. Mech. Engrs* **38**, 409–434.
- [10] LANNES, D. 2013 *The Water Waves Problem*. American Mathematical Society.
- [11] LI, Y. & ELLINGSEN, S. 2016 Ship waves on uniform shear current at finite depth: wave resistance and critical velocity. *J. Fluid Mech.* **791**, 539–567.
- [12] LUSTRI, C. J. & CHAPMAN, S. J. 2013 Steady gravity waves due to a submerged source. *J. Fluid Mech.* **732**, 660–686.
- [13] MIAO, S. & LIU, Y. 2015 Wave pattern in the wake of an arbitrary moving surface pressure disturbance. *Phys. Fluids*. **27** (12).
- [14] NOBLESSE, F., HE, J., ZHU, Y., HONG, L., ZHANG, C. AND ZHU, R. & YANG, C. 2014 Why can ship wakes appear narrower than Kelvin’s angle? *Euro. J. Mech-B* **46**, 164–171.
- [15] PEDERSEN, G. 1988 Three-dimensional wave patterns generated by moving disturbances at transcritical speeds. *J. Fluid Mech.* **196**, 39–63.
- [16] PETHIYAGODA, R., McCUE, S. W. & MORONEY, T. J. 2014 What is the apparent angle of a Kelvin ship wave pattern? *J. Fluid Mech.* **758**, 468–485.
- [17] PETHIYAGODA, R., MORONEY, T. J., LUSTRI, C. J. & McCUE, S. W. 2021 Kelvin wake pattern at small froude numbers. *J. Fluid Mech.* **915**, A126.
- [18] RABAUD, M. & MOISY, F. 2013 Ship wakes: Kelvin or mach angle? *Phys. Rev. Lett.* **110** (21), 214503.
- [19] TRINH, P. H. & CHAPMAN, S. J. 2014 The wake of a two-dimensional ship in the low-speed limit: results for multi-cornered hulls. *J. Fluid Mech.* **741**, 492–513.
- [20] TRINH, P. H., CHAPMAN, S. J. & VANDEN-BROECK, J-M. 2011 Do waveless ships exist? results for single-cornered hulls. *J. Fluid Mech.* **685**, 413–439.
- [21] ȚUGULAN, C., TRICHTCHENKO, O. & PĂRĂU, E. I. 2022 Three-dimensional waves under ice computed with novel preconditioning methods. *J. Comp. Phys.* **459**, 111129.
- [22] WHITHAM, G. B 1974 *Linear and nonlinear waves*. John Wiley.
- [23] ZHANG, Z., YANG, X., GUO, Q. & CAO, Y. 2023 Rare decaying ripple solutions within the KP equation. *Physica D* **456**, 133920.